

Contents lists available at [ScienceDirect](#)

Applied Geochemistry

journal homepage: www.elsevier.com/locate/apgeochem

Oxygen influx and geochemistry of percolate water from reactive mine waste rock underlying a sloping channelled soil cover

Qing Song*, Ernest K. Yanful

Geotechnical Research Center, Department of Civil and Environmental Engineering, University of Western Ontario, 1151 Richmond Street, London, ON, Canada N6A 5B9

ARTICLE INFO

Article history:

Received 12 March 2010
 Accepted 5 January 2011
 Available online xxxx
 Editorial handling by LeeAnn Munk

ABSTRACT

An ideal engineered soil cover can mitigate acid rock drainage (ARD) by limiting water and gaseous O₂ ingress into an underlying waste rock pile. However, the barrier layer in the soil cover almost invariably tends to develop cracks or fractures after placement. These cracks may change water flow and O₂ transport in the soil cover and decrease performance in the long run. The present study employed a 10-cm-wide sand-filled channel installed in a soil barrier layer (silty clay) to model the aggregate of cracks or fractures that may be present in the cover. The soil cover had a slope of 20%. Oxygen transport through the soil cover and oxidation of the underlying waste rock were investigated and compared to a controlled column test with bare waste rock (without soil cover). Moreover, gaseous O₂ transport in the soil cover with channel and its sensitivity to channel location as well as the influence of the saturated hydraulic conductivity of the channel material were modeled using the commercial software VADOSE/W. The results indicated that the waste rock underlying the soil cover with channel had a lower oxidation rate than the waste rock without cover because of reduced O₂ ingress and water flushing in the soil cover with channel, which meant a partial soil cover might still be effective to some extent in reducing ARD generation. Gaseous O₂ ingress into the covered waste rock was more sensitive to the channel location than to the saturated hydraulic conductivity of the material filling the channel. Aqueous equilibrium speciation modeling and scanning electron microscopy with energy dispersive X-ray analysis indicated that secondary minerals formed as a result of the oxidation of the waste rock included gypsum and goethite in the covered waste rock and schwertmannite and other Fe oxides in the uncovered waste rock. The findings of the study provided insight into the effect of channel flow on O₂ transport and oxidation of the covered waste rock, which may help to improve soil cover design and construction to minimise the generation of preferential flow in the barrier layer.

© 2011 Elsevier Ltd. All rights reserved.

1. Introduction

The diffusion coefficient of gaseous O₂ in water is much smaller than in air, therefore, the gaseous O₂ flux through an engineered soil cover into the underlying reactive waste rock could be reduced significantly when the barrier layer in the soil cover maintains high water saturation (Nicholson et al., 1989; Yanful, 1993; O'Kane et al., 1998). As a result, a lot of research has focused on maintaining high saturation in the barrier layer in resistive soil covers. Among the research topics studied, the capillary barrier effect, which is produced by placing a fine-grained material over a coarse-grained material, has probably received the most attention over the years. The capillary barrier concept is usually employed in soil cover design to meet the high saturation requirement of the barrier layer (e.g. Aubertin et al., 1994; Woyschner and Yanful,

1995; Yanful et al., 2003; Weeks and Wilson, 2005; Bussière et al., 2007). The water content of the barrier layer can be influenced by a number of factors including soil properties, climatic conditions, soil cover configuration, and the geometry of the soil cover. For example, Bussière et al. (2003) investigated an inclined soil cover and found that the upslope section of the cover had a lower saturation than the downslope. Stormont (1996) found that a layered capillary barrier was more effective than a homogeneous capillary barrier at the same slope of 10%.

Preferential flow in a soil cover can also influence the water content of the barrier layer. Water flow in macropores (Beven and Germann, 1982), fingered flow (Hill and Parlange, 1972; Selker et al., 1992), and funnel flow (Kung, 1990; Walter et al., 2000) are three different preferential flow mechanisms. Among them, water flow in macropores is the main concern related to the soil cover performance and is the subject of the present study. Beven and Germann (1982) reviewed factors that cause the formation of macropores in soils. These factors include soil fauna, plant roots, desiccation, freeze–thaw cycles, and subsurface flow erosion.

* Corresponding author. Tel.: +1 519 661 3344; fax: +1 519 661 3942.

E-mail addresses: qsong3@uwo.ca, jasonsong702@yahoo.ca (Q. Song), eyanful@eng.uwo.ca (E.K. Yanful).

Preferential flow has also been found to occur in soil covers in the field by several researchers. For example, Taylor et al. (2003) reported that infiltration increased and soil cover performance decreased at the Rum Jungle mine site in Australia after 10 a due to shrinkage, plant root penetration and animal invasion. Adu-Wusu and Yanful (2006) found that preferential flow occurred in pilot test soil covers incorporating geosynthetic clay liner and sand-bentonite mixture as barrier materials in the third year at the Whistle mine site in Canada. Although preferential flow has been found to impact infiltration or percolation in soil covers in the field, little has been done in the laboratory to examine the effect of preferential flow on soil cover performance, especially O₂ transport in the soil cover. A laboratory study offers better control of influencing factors and allows an evaluation of the effect of each factor on cover performance indicators such as water balance, O₂ ingress and residual oxidation of the covered waste.

In the present study, a soil cover (Test 1) consisting of sand and silty clay was installed over reactive mine waste rock in the laboratory. A 10-cm-wide channel filled with sand was installed in the silty clay layer to simulate preferential flow (referred to as channel flow in this paper) in the barrier layer. The purpose of the experiment (Test 1 or cover with channel) was to investigate the effect of channelling on water balance, O₂ transport and waste rock oxidation. The sand-filled channel was designed to represent the aggregate of fissures and/or cracks that frequently develop in compacted clayey soils used as barrier layers. The macroporosity of the channel with respect to the silty clay layer was 3.4%, and the macropores in the channel accounted for 10.4% of pore volume of the silty clay layer. The configuration of the channel used in the experiment is not uncommon with respect to preferential flow pathways occurring in field soils. Song and Yanful (2010a) discussed the channel configuration in detail and showed that the channel macroporosity of 3.4% was similar to values for macropore networks studied by other researchers (e.g. Germann and Beven, 1981; Zehe and Flüher, 2001). Measurements and modeling of the impact of the channel on the water balance for the cover have been presented by Song and Yanful (2010a,b). The present study deals with O₂ influx to the waste rock with channelled cover and the geochemistry of the resulting percolate water from Test 1. For comparison, a column test (Column 1 or waste rock without cover) was also set up to investigate waste rock oxidation. The column test had the same rainfall frequency and intensity as the covered waste rock. Although two tests had different scales, this comparison can still provide information on how the presence of the channel pathway influenced oxidation of the underlying waste rock.

A commercial finite element software, VADOSE/W (GEO-SLOPE, 2004), was used to model the distribution of O₂ in the waste rock in Test 1. It was also used to further analyze the effects of the location of the channel and the saturated hydraulic conductivity of the fill material on O₂ concentration and O₂ flux through the soil cover. The aqueous equilibrium speciation program, PHREEQC (Parkhurst and Appelo, 1999), was employed to investigate the geochemistry of percolate waters from Test 1 and Column 1. The objectives of the present paper are (1) to present the oxidation characteristics of the covered waste rock (Test 1) and uncovered waste rock (Column 1); (2) to model the distribution of O₂ in the waste rock with the sloping, channelled cover (Test 1); and (3) to present the effects of the location of the channel and the saturated hydraulic conductivity of the channel filling material on O₂ transport.

The same computer program VADOSE/W has been used by the authors (Song and Yanful, 2010b) to model the hydrogeological behaviour of the same channelled cover (i.e., Test 1). During the water flow modeling, hydraulic properties (such as the soil-water characteristic curve and unsaturated hydraulic conductivity functions) of the materials were calibrated using a step-by-step ap-

proach. The hydrogeological modeling results indicated that percolation was sensitive to both the channel location and the saturated hydraulic conductivity of channel filling material. The successful hydrogeological modeling provided a foundation to further evaluate the influence of channelled cover on gaseous O₂ flux because the gaseous O₂ flux is intrinsically affected by water movement in the cover. Oxygen influx and geochemical speciation modeling in the present study could provide further understanding of the influence of the channelled cover on gaseous O₂ transport in the cover and hence on the geochemistry of the infiltrated waters draining the underlying sulfidic waste rock. Thus the present work differs from but builds on the two previous papers published by the authors (Song and Yanful, 2010a,b).

2. Materials and methods

2.1. Materials

Materials used in the experiments included waste rock, silty clay and construction sand. The waste rock was obtained from the Matabi mine site near Ignace, Ontario, Canada. Before its use in the experiments, the waste rock was crushed, sieved, and washed. The crushed particle size of the waste rock was less than 12.5 mm (passing No. ½ in. sieve). The waste rock contained sulfide-bearing minerals including pyrite, sphalerite, chalcopyrite and pyrrhotite, and gangue minerals such as quartz, clinocllore, muscovite and mica. The silty clay and sand were obtained from a suburb of London, Ontario, Canada. The dominant minerals in the sand were quartz, dolomite, and calcite. The silty clay comprised mainly quartz, calcite, dolomite, illite and chlorite. The most abundant elements in the waste rock included Fe (18.6%), S (17.6%), Zn (3.6%), Ca (0.9%) and Al (0.6%). The most abundant elements in the silty clay were Ca (11.8%), Fe (1.7%), Al (1%) and S (0.2%). The most abundant elements in the sand were Ca (19.6%), Fe (0.8%), Al (0.3%) and S (0.1%). The detailed elemental composition and geotechnical properties of the test materials have been presented by Song and Yanful (2010a).

2.2. Experiment setup

The experimental unit used in Test 1 (waste rock with the sloping channelled soil cover) was a plastic box measuring 120 cm × 120 cm × 25 cm (width × height × thickness). The box was placed on a steel frame. A rainfall distributor installed above the box during wetting periods was designed to simulate precipitation. There were two outlets attached to the sidewall of the box to collect runoff and interflow and three outlets at the bottom to collect percolation. The test materials were placed in the box in layers. The surface of the waste rock layer had a slope of 20%, so the height of the waste rock ranged from 11 cm at the lowest point to 35 cm at the highest point. The compacted silty clay layer and uncompacted sand layer were 50 cm and 30 cm in height, respectively. The silty clay was compacted as a 5-cm-thick sublayer at a time outside the box and was then moved and placed in the box. The water content of the silty clay layer was controlled at 2% above the optimum water content (15.8%) during the compaction. A 10-cm-wide channel filled with the same sand as the overlying sand layer was installed in the silty clay layer. The channel was located 30 cm from the highest point of the soil cover. The section of the soil cover in the box is shown in Fig. 1a. The porosity of the sand, silty clay, and waste rock in Test 1 was 0.41, 0.36 and 0.26, respectively. Fig. 1a also shows the O₂ sampling ports in the soil cover in Test 1. In total, 11 oxygen sampling ports were installed in the soil cover. Water traps (not shown in Fig. 1a) were installed in Outlets 2–5 to prevent gaseous O₂ from entering, from side and bottom of

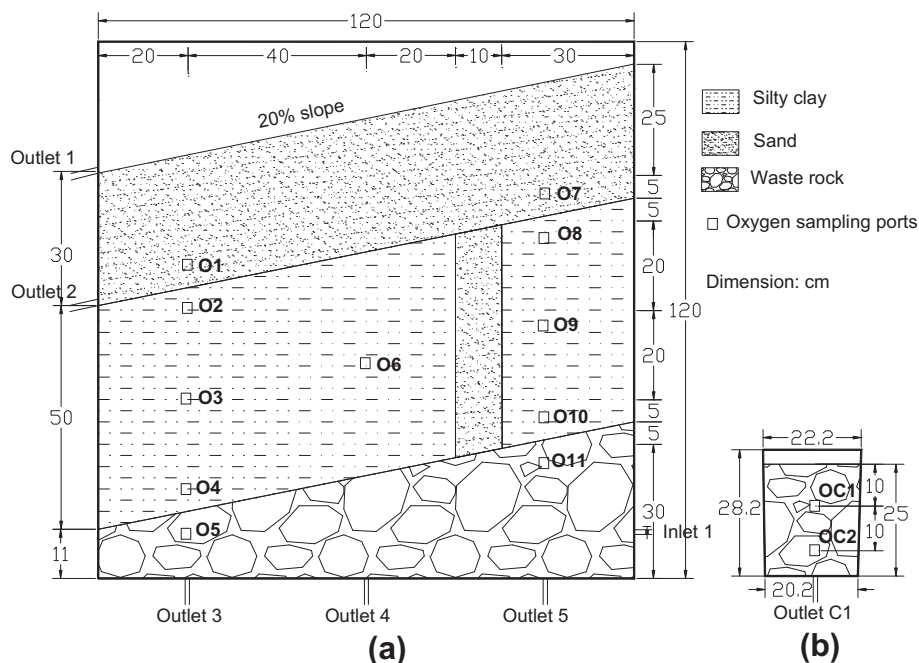


Fig. 1. (a) Vertical section of the test soils and instrumentation in Test 1 (waste rock with channelled cover); (b) vertical section of Column 1 (waste rock without cover).

the box, into the waste rock layer. A rubber stopper (not shown in Fig. 1b) was used to avoid gaseous O_2 entering into the waste rock from the bottom Outlet C1 in Column 1.

The tapered column used in Column 1 measured 20.2 cm in diameter at the bottom, 22.2 cm at the top, and 28.2 cm in height (Fig. 1b). The column was sealed at the bottom with a 6-mm diameter outlet for effluent collection. The height of the waste rock in the column was 25 cm, which was similar to the average height (23 cm) of the waste rock in Test 1. Two O_2 sampling ports located 10 cm apart were installed in Column 1. The dry density of the waste rock in Column 1 was 2.06 g/cm^3 , and the porosity was 0.27. This porosity was slightly different from the porosity (0.26) of the waste rock placed in Test 1. This minor discrepancy was probably due to errors associated with the installation of the test units (such as weighing accuracy) of the waste rock. The waste rock was homogenized before being used in the experiments.

2.3. Measurements

Extensive measurements were carried out in Test 1 to obtain a number of parameters including soil temperature, suction, water content, runoff, interflow, percolation, precipitation and O_2 concentration (Song and Yanful, 2010a). Precipitation, percolation and O_2 concentration in Column 1 were also measured. The O_2 sampling ports incorporated rubber septa that automatically sealed after drawing a sample of air using a syringe with a needle. A volume of 2-mL of air was extracted from the O_2 sampling port and injected into an O_2 analyzer (Quantek Instruments, Model 905V) to measure the O_2 concentration. The O_2 analyzer was calibrated in the atmosphere before each sampling. The O_2 concentration in the experiments was monitored every 3 days.

A number of chemical parameters for the percolate waters from Test 1 and Column 1 were measured, which included pH, Eh (redox potential), electrical conductivity, acidity, alkalinity, SO_4^{2-} concentration and dissolved metal concentrations. Percolate water pH was measured using an ORION 410A pH meter (Thermo Scientific), and electrical conductivity and Eh were measured with a multi-parameter handheld meter (WTW, Multi 340i). Acidity and alkalinity

were measured by titration with 0.01 N NaOH and 0.02 N H_2SO_4 , respectively, through an automated titration device (Metrohm AG, 785 DMP Titrino). The SO_4^{2-} concentration of the percolate water was measured using a high performance liquid chromatography (HPLC) system (Waters Corporation, Waters 432 Conductivity Detector). Dissolved metal ions were determined using inductively coupled plasma-optical emission spectrometry (ICP-OES) (Varian Inc., Vista-Pro).

The precipitation frequency employed in the experiments was to simulate drying and wetting cycles at Whistle mine site, near Capreol, Ontario, Canada. The precipitation intensity for Test 1 and Column 1 was the same. Fig. 2 presents the precipitation intensity and water amount added in Test 1 and Column 1. The test period was from February 8 to July 8, 2008 for Test 1 and from February 25 to July 25, 2008 for Column 1. Air temperature and relative humidity in the laboratory were also recorded during the experiments.

2.4. Acid base accounting test

An acid base accounting (ABA) test was employed in the study to evaluate the acid generating or neutralizing potential of the waste rock. The ABA test includes the measurement of neutralization potential (NP) and acid generation potential (AP). The susceptibility of the waste rock to acid generation is determined based on the difference between NP and AP or the ratio of NP to AP. The difference between NP and AP is called the net neutralization potential (NPP), that is, $NPP = NP - AP$, while the ratio of NP to AP is the neutralization potential ratio (i.e. $NPR = NP/AP$). If the NNP value is less than $-20 \text{ kg CaCO}_3/\text{tonne}$, the material is a potential acid producer. The material is not likely to form acid if the NNP value is greater than $20 \text{ kg CaCO}_3/\text{tonne}$. For NNP value between -20 and $20 \text{ kg CaCO}_3/\text{tonne}$, it is difficult to determine the acid potential just from the ABA test results (USEPA, 1994). In the present study, the ABA test was performed according to the modified Sobek method (MEND, 1991). The AP was calculated from the amount of sulfide-S, which was the difference between total S and SO_4-S .

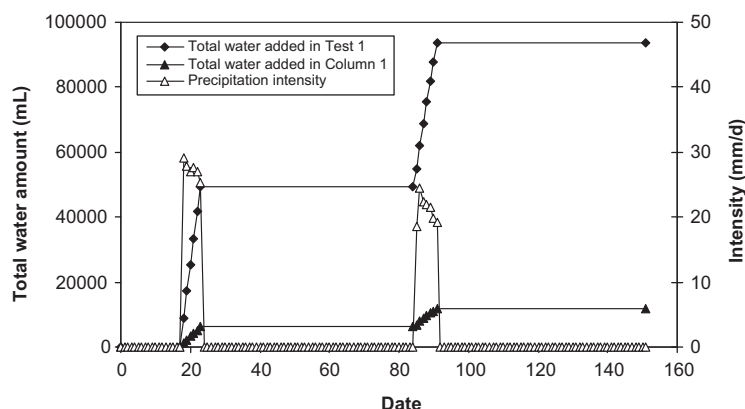


Fig. 2. Water amount added in Test 1 (waste rock with channelled cover) and Column 1 (waste rock without cover) and precipitation intensity.

2.5. Oxygen transport in VADOSE/W

Oxygen transport is simulated in the program VADOSE/W (Eq. (1)) by accounting for O_2 diffusion in both air and water phases and for decay (Krahn, 2004):

$$\frac{\partial(\theta_{eq}C)}{\partial t} = D_{eff} \frac{\partial^2 C}{\partial x^2} + D_{eff} \frac{\partial^2 C}{\partial y^2} - \lambda^* \theta_{eq} C \quad (1)$$

where C is the pore gas O_2 concentration, θ_{eq} is the effective porosity, D_{eff} is the effective diffusion coefficient, and λ^* is the bulk O_2 decay coefficient. The effective porosity is defined as Eq. (2) (Aubertin et al., 2000).

$$\theta_{eq} = \theta_a + H_c \theta_w \quad (2)$$

where θ_a is the volumetric air content (or air filled porosity), θ_w is the volumetric water content, H_c is the dimensionless Henry's equilibrium constant (H_c is approximately 0.03 at 20 °C). The bulk O_2 decay coefficient, λ^* , is defined as

$$\lambda^* = \frac{\ln 2}{t_{1/2}^*} \quad (3)$$

where $t_{1/2}^*$ is the half-life of the O_2 decay.

During modeling, the program can calculate D_{eff} using the method of Collin and Rasmuson (1988) based on the simulated saturation. The half-life $t_{1/2}^*$ is an input parameter. Eqs. (1) and (2) show that O_2 transport and O_2 distribution in the soil cover are dependent on water flow. However, water flow is independent of O_2 transport during the flow modeling, which provides a convenient way to calibrate relevant parameters to O_2 transport, especially, the half-life of O_2 (or the bulk decay coefficient) due to O_2 consumption. Except for the upper boundary, all other boundary conditions in the O_2 transport modeling were set as zero flux. The upper boundary was the climatic boundary. The initial O_2 concentration in the model was set to 180 g/m³ for all nodes. This value was close to the measured O_2 concentration of 13.6% at the beginning of the test. The half-life of the O_2 decay in the waste rock was set to 0.005 a (the optimum value for the tested waste rock obtained from model calibration).

As mentioned above, the modeling of water balance in Test 1 provided a basis for the modeling of O_2 transport. Just like the water balance (Song and Yanful, 2010b), the modeling of O_2 influx in the present study also involved two stages. The first stage was to calibrate the half-life or bulk O_2 decay coefficient. This was done by fitting the simulated O_2 concentrations in the cover soils (mainly silty clay) and the waste rock to the measured results in Test 1 (cover with channel). It should be noted that this method of obtaining the half-life or bulk O_2 decay coefficient was evaluated by comparison with the SO_4^{2-} release method and with other published methods in a previous publication (Song and Yanful, 2010c).

After obtaining the bulk O_2 decay coefficient, the effects of location of the channel pathway and saturated hydraulic conductivity of the channel filling material on O_2 transport in the cover were modeled. The location of the channel pathway was expressed as a normalized distance (x), defined as the ratio of the horizontal distance between the mid-point of the channel pathway and the highest point of the soil cover to the total horizontal length of the soil cover. Therefore, the normalized distance will increase with the location of the channel pathway moving from upslope to downslope of the soil cover. When investigating the effect of the saturated hydraulic conductivity of the channel filling material on O_2 transport, the channel pathway was set at the same position as built in Test 1 (i.e. $x = 0.29$). Table 1 lists the cases modeled in the present study.

2.6. Geochemical speciation modeling

The difference between the oxidation rate of the covered waste rock (Test 1) and that of the uncovered waste rock (Column 1) could produce drainage with different water chemistry and, possibly, different secondary minerals. The ion speciation model PHREEQC (Parkhurst and Appelo, 1999) was employed to assess the possible formation or dissolution of secondary minerals based on the water chemistry data from the effluents (final effluents) in Test 1 and Column 1. One of the outputs from PHREEQC is the saturation index (SI) of individual potential minerals calculated as

$$SI = \log_{10} \left(\frac{IAP}{K_{so}} \right) \quad (4)$$

where IAP is the ion activity product of a mineral, K_{so} is the equilibrium constant or solubility constant. The SI value is an indication of the mineral's potential state in the water. The thermodynamic database in Minteq v4 (USEPA, 1999) was used for the modeling. Schwertmannite ($Fe_8O_8(OH)_6SO_4$) solubility constant of $\log K_{so} = 18.0$ (Bigham et al., 1996) and enthalpy of -452.7 kJ/mol modified from Majzlan et al. (2004) were added to the database. The input data used in PHREEQC modeling are listed in Table 2. The data represent values for effluents or drainage waters obtained at the end of the test since the geochemistry of the last extraction would reflect the final status of the waste rock in the two tests. This final status would provide information on possible secondary mineral precipitation or dissolution.

2.7. Secondary mineral identification

Scanning electron microscopy (SEM) with energy dispersive X-ray analysis (EDX) was employed to confirm the formation of secondary minerals predicted by PHREEQC. Samples of waste rock obtained after the tests were divided into six groups according to

Table 1
Modeling cases to investigate the effect of channel flow on O₂ transport through the soil cover.

Modeling case	Type of case	Purpose	Properties of the channel pathway	
			Normalized distance ^a , x, (m/m)	Saturated hydraulic conductivity (m/day)
Case 1	Experimental test (Test 1)	To calibrate model	0.29	24.2
Case 2	Hypothetical case	To evaluate the effect of the location of the channel pathway on oxygen influx	0.04	24.2
Case 3	Hypothetical case		0.54	24.2
Case 4	Hypothetical case		0.71	24.2
Case 5	Hypothetical case		0.96	24.2
Case 6	Hypothetical case	To evaluate the effect of hydraulic conductivity of channel material on oxygen influx	0.29	242
Case 7	Hypothetical case		0.29	121
Case 8	Hypothetical case		0.29	48.4
Case 9	Hypothetical case		0.29	12.1
Case 10	Hypothetical case		0.29	4.84
Case 11	Hypothetical case		0.29	2.42

^a Normalized distance (x) is the ratio of the horizontal distance from the mid-point of the channel to the highest point on the soil cover over the total horizontal length of the cover.

Table 2
Input data (measurements obtained from the final effluents) used in PHREEQC modeling.

Identifier	Test 1 ^a (mg/L, except for pH and pe)	Column 1 ^b (mg/L, except for pH and pe)
pH	7.6	6.7
Pe	3.8	4.7
Al	1.39×10^{-2}	9.31×10^{-2}
Sb	1.29×10^{-2}	3.98×10^{-3}
As	6.01×10^{-3}	4.10×10^{-3}
Ba	2.24×10^{-2}	8.51×10^{-3}
Cd	7.51×10^{-4}	6.67×10^{-2}
Ca	5.99×10^2	6.44×10^2
Co	1.64×10^{-3}	2.36×10^{-2}
Cu	2.45×10^{-3}	5.84×10^{-2}
Fe	9.26×10^{-2}	3.87×10^{-2}
Pb	1.72×10^{-2}	8.63×10^{-2}
Mg	6.78×10^1	4.95×10^1
Mn	4.86×10^0	5.80×10^0
Ni	6.55×10^{-3}	7.63×10^{-2}
K	2.45×10^1	4.43×10^0
Se	8.33×10^{-3}	9.90×10^{-2}
Si	3.45×10^1	1.85×10^1
Na	1.21×10^1	2.84×10^0
Sr	1.12×10^0	5.97×10^{-1}
SO ₄ ²⁻	1.48×10^3	1.39×10^3
Zn	8.96×10^{-1}	1.86×10^1
Alkalinity (as CaCO ₃)	$1.69 \times 10^{+2}$	1.91×10^1

^a Test 1: Waste rock with channelled cover.

^b Column 1: Waste rock without cover.

the extent of oxidation identified visually. Sub-samples identified visually to be the mostly severely oxidized were used for analysis. The mounted samples for SEM analysis were coated with Au. The mineral chemistry was determined using the Hitachi 3400-N variable pressure scanning electron microscope (VP-SEM) equipped with an EDX spectrometer at 12 kV accelerating voltage. The minerals were confirmed by normalized weights of the detected elements in the scanned area and the crystals in the image combined with the output from the PHREEQC modeling.

3. Results

3.1. Acid base accounting test results

The paste pH of the waste rock was 5.8. Total S (mainly from pyrite and sphalerite) accounted for 19.7% and the SO₄-S was

0.5%, so the calculated AP (acid generation potential) was 600 kg CaCO₃ equivalent per tonne of the waste rock. The NP (neutralization potential, mainly produced by calcite) was 29 kg CaCO₃ equivalent per tonne of the waste rock. As a result, the waste rock had a net neutralization potential (NNP) of -571 kg CaCO₃ equivalent per tonne and was, therefore, identified to be a potential acid producer.

3.2. Results of measured and modeled oxygen concentrations

Fig. 3 shows the measured O₂ concentration profiles at the downslope section (O1–O5) in Test 1. During rainfall events (e.g. May 8, 2008), the O₂ sampling ports O1, O2 and O3 were filled with water (hence zero readings were recorded). However, O₂ concentrations at O4 and O5 were almost the same, approximating 6.5%. During drying periods, the O₂ concentration in the sand layer (O1) was approximately 20.8%, which was close to the atmospheric O₂ concentration (20.9%). Oxygen concentrations in the silty clay layer decreased with depth. For example, the O₂ concentration was 13.5% at O3 and 10.6% at O4 on April 8, 2008. Sampling port O2 was filled with water following the first rainfall events, therefore the O₂ concentration at this point was not available. Oxygen concentrations at O5 were relatively stable with a value of approximately 11.5% in the dry periods. For a particular time, the O₂ concentration at O4 (in the silty clay) was close to or even lower than the O₂ concentration at O5 (in the waste rock), implying that gaseous O₂ was not transported from O4 to O5 in Test 1. This phenomenon was attributed to the presence of the sand-filled channel in the silty clay layer. Gaseous O₂ would have been transported more easily through the sand-filled channel to arrive in the underlying waste rock layer than through the silty clay layer because the sand in the channel would have a higher diffusion coefficient than the silty clay (Song and Yanful, 2010a).

During the rainfall events (Day 85–91) shown in Fig. 4, the measured and modeled O₂ concentrations in the waste rock decreased quickly, but then increased steadily in the drying periods. The measured O₂ concentrations downslope (O5) in the waste rock were between 6.2% and 12.1%, and the modeled O₂ concentrations at the same location ranged from 5.2% to 11.5%; thus the modeled O₂ concentration matched the measured results very well at the downslope section (O5) of the waste rock. Similarly, the modeled O₂ concentrations (6.7–14.2%) upslope (O11) in the waste rock agreed well with the measured values (7.8–14.7%). Therefore, VA-DOSE/W provided reasonable predictions of gaseous O₂ transport

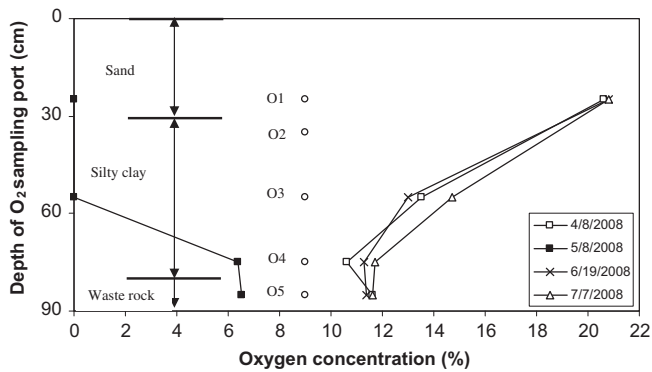


Fig. 3. Measured O_2 concentration profiles downslope in Test 1 (waste rock with channelled cover) at the selected time (O1–O5 are the O_2 sampling ports). Oxygen concentrations in O2 were not available due to water filling in the port.

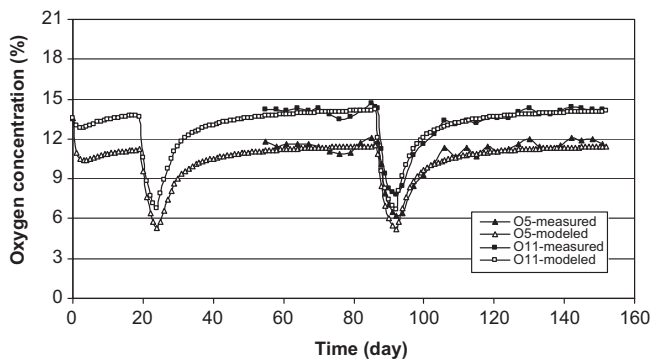


Fig. 4. Measured and modeled O_2 concentrations in the waste rock (O5 at the downslope section of the soil cover; O11 at the upslope section of the soil cover). Dips denote the end of rainfall events.

when the optimum O_2 consumption half-life value (0.005 a) was input in the modeling.

The modeled O_2 concentrations in the waste rock downslope (O5) and upslope (O11) at different locations of the channel pathway are shown in Figs. 5a and 5b, respectively. First of all, the modeled O_2 concentration at both locations O5 and O11 decreased significantly during the rainfall events and then increased steadily in the following drying periods. Secondly, the distribution of gaseous O_2 concentration in the waste rock depended on the location of the channel pathway. Closer to the channel, higher O_2 concentrations occurred. When the location of the channel pathway changed from the downslope section to the upslope section of the soil cover (i.e. x decreased), the O_2 concentration decreased at the downslope section (O5) and increased at the upslope section (O11). For example, the O_2 concentration values at the end of the modeling period were 13.9% at O5 and 10.1% at O11, respectively, for $x = 0.71$ (Case 4) and 9.9% at O5 and 13.5% at O11, respectively, for $x = 0.04$ (Case 2). Due to the influence of the slope of the soil cover on the water content of the channel sand, the modeled gaseous O_2 concentrations at O5 or O11 were different even if the distance between the channel and the modeled point was the same. For example, in Case 4 ($x = 0.71$) and Case 5 ($x = 0.96$) the channel pathway had the same distance to O5, but the O_2 concentrations at the end of the modeling period were 13.9% in Case 4 and 12.3% in Case 5. Similar results can be found at O11 with an O_2 concentration of 14.1% in Case 1 ($x = 0.29$) and 13.5% in Case 2 ($x = 0.04$).

Fig. 6 shows the modeled O_2 concentrations in the waste rock (O5 and O11) when the channel pathway location was kept the same as the experimental case ($x = 0.29$), but the saturated hydraulic

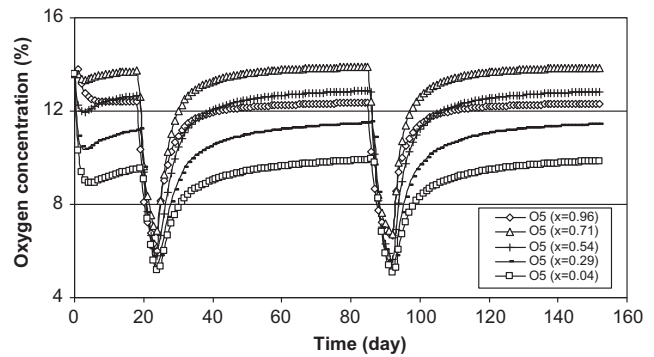


Fig. 5a. Modeled O_2 concentrations in the waste rock downslope (O5) when the channel pathway is at the different locations (x is the normalized distance of the channel pathway).

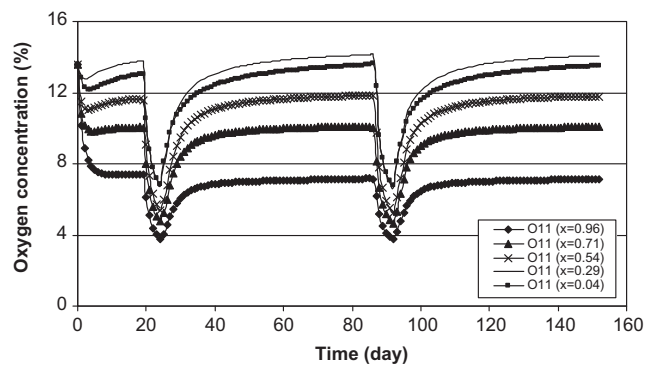


Fig. 5b. Modeled O_2 concentrations in the waste rock upslope (O11) when the channel pathway is at the different locations (x is the normalized distance of the channel pathway).

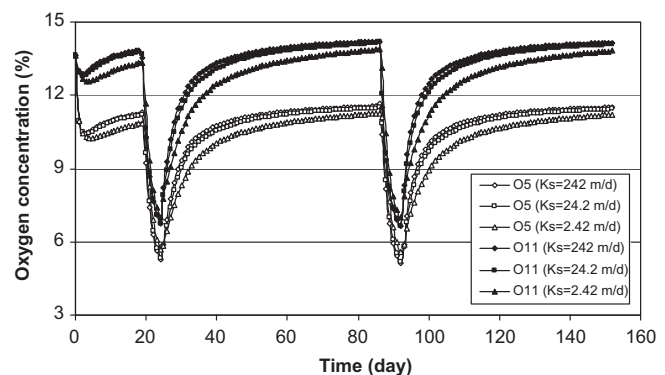


Fig. 6. Modeled O_2 concentrations in the waste rock when changing the saturated hydraulic conductivity of the channel filling material (O5 at the downslope section of the soil cover, O11 at the upslope section of the soil cover).

lic conductivity (K_s) of the channel filling sand was varied. Only the modeled O_2 concentrations obtained from Case 1, Case 6 and Case 11 are presented because other hypothetical cases gave similar results. Fig. 6 indicates that O_2 concentrations at O5 and O11 have the same trends when K_s of the channel material is varied. With increase in K_s , the O_2 concentration at O5 and O11 increased slightly, and most of the increase occurred at the beginning of the drying period. At the end of the drying period, the O_2 concentrations became close to each other for different saturated hydraulic conductivity values. For example, O_2 concentrations at O5 on Day 104 were 10.5% in Case 6 ($K_s = 242$ m/day) and 9.6% in Case 11

($K_s = 2.42$ m/day), but on Day 152 the O_2 concentrations were 11.5% in Case 6 and 11.2% in Case 11. Similar results were found at O11. Fig. 6 also shows that the O_2 concentration upslope (O11) was higher (approximately 2.6%) than the value downslope (O5) in the drying periods for each saturated hydraulic conductivity of the channel material. During rainfall events, the O_2 concentration at O5 and O11 decreased significantly. However, the rainfall events caused a larger decrease in the O_2 concentration at O11 than at O5 because of the proximity of the channel to O11.

Fig. 7 shows the cumulative O_2 flux into the waste rock layer for various locations of the channel pathway. The O_2 flux increased when the channel pathway moved from the downslope section to the upslope section of the soil cover (i.e. the normalized distance of the channel pathway, x , decreased). At $x = 0.29$ (Case 1), the maximum cumulative O_2 flux was calculated to be 102 g. The O_2 flux decreased sharply when the channel was very close to the upslope boundary. Since the O_2 decay coefficient was the same for the all modeled cases, the difference in the cumulative O_2 flux was mainly caused by the difference in the O_2 diffusion coefficients resulting from the variable water contents in the cover soils, especially in the channel pathway. Because the total modeling time was the same for each modeling case, the average daily O_2 flux was expected to have a similar relationship to the location of the channel pathway, as the cumulative O_2 flux did. The upslope and downslope boundaries may, to some extent, influence O_2 flux because gaseous O_2 had a longer transport pathway with the channel close to the boundaries than with the channel at other locations. The modeled cumulative gaseous O_2 flux into the underlying waste rock without channel (i.e. an intact cover) was 0.34 g over the same period (151 days).

The cumulative O_2 influx increased with an increase in the saturated hydraulic conductivity of the channel filling material (Fig. 8), but the difference in O_2 influx among the modeled cases was not significant. For example, the cumulative O_2 flux was 100 g for $K_s = 2.42$ m/day (Case 11) and 104 g for $K_s = 242$ m/day (Case 6). Again, these small differences in the cumulative O_2 influx may be attributed to the different O_2 diffusion coefficients resulting from the difference in water contents. Based on the modeled O_2 distribution in the waste rock (Fig. 6) and the modeled O_2 influx into the waste rock (Fig. 8), it can be inferred that the performance of the soil cover may reduce significantly when a channel pathway develops in the barrier layer. The hydraulic properties of the channel filling sand and silty clay showed that the air entry value was 0.4 kPa for sand and 80 kPa for silty clay, and the saturated hydraulic conductivity was 24.2 m/day for sand and 0.000082 m/day for silty clay. This hydraulic contrast between the channel filling sand and silty clay resulted in the calculated effective O_2 diffusion coef-

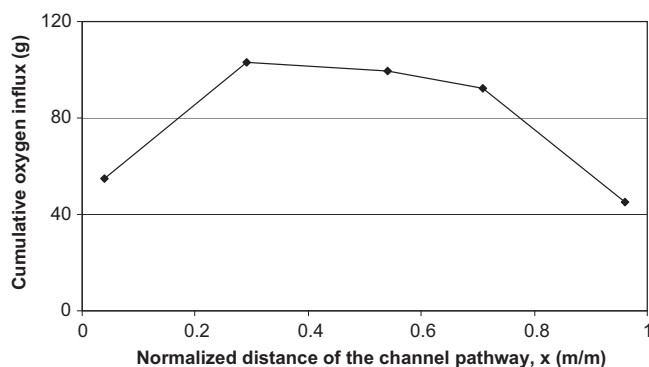


Fig. 7. Relationship between the modeled cumulative O_2 influx to the underlying waste rock and the location of the channel in the silty clay layer (Cases 1–5).

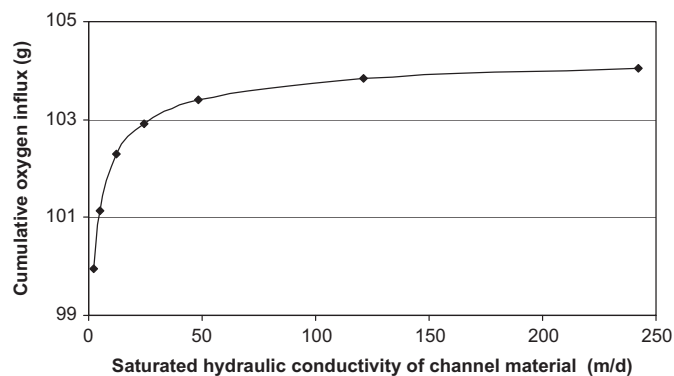


Fig. 8. Relationship between the cumulative O_2 influx to the waste rock and the saturated hydraulic conductivity of the material filling the channel pathway (Case 1 and Cases 6–11).

cient of 8.0×10^{-6} m²/day for the silty clay and 2.8×10^{-1} m²/day for the channel sand (Song and Yanful, 2010a).

Measured O_2 concentrations from two O_2 sampling ports in Column 1 (waste rock without cover) had a value of approximately 20.7%, which was close to the O_2 concentration in the atmosphere. As a result, it was impossible to estimate O_2 flux from the measured O_2 concentration profile in Column 1.

3.3. Percolate water geochemistry in Test 1 and Column 1

The measured pH of the percolate water in Test 1 (waste rock with channelled cover) was higher than that in Column 1 (waste rock without cover) as shown in Fig. 9. For example, the pH values of the percolate water in Test 1 ranged from 6.6 to 7.8, while values in Column 1 were between 6.1 and 6.7. There may be two reasons for the difference: (1) the covered waste rock in Test 1 oxidized more slowly than the uncovered waste rock in Column 1; (2) the drainage from the overlying soil cover layers (mostly from the sand) in Test 1 had a higher pH value and could have neutralized the pore water in the waste rock in Test 1. For example, the paste pH was 8.3 for the sand, 7.6 for the silty clay and 5.8 for the waste rock. The pH of the percolate water in both Test 1 and Column 1 decreased significantly at Day 85 due to increased oxidation resulting from the long drying period.

After the second rainfall events (Day 92), the mass of cumulative SO_4^{2-} released from the waste rock was 907 mg/kg in Column 1 and 530 mg/kg in Test 1 (Fig. 9), and the corresponding oxidation rate was 8.6 mg (SO_4^{2-})/kg/day in Column 1 and 5.0 mg (SO_4^{2-})/kg/day (ignoring the packing period) in Test 1. It should be noted that the measured cumulative SO_4^{2-} release rate in Test 1 was probably underestimated due to the precipitation of a secondary mineral, such as gypsum, compared to the calculated O_2 influx. Based on the modeled O_2 influx, there was a total of 102 g of gaseous O_2 ingress into the underlying waste rock during 151 days of testing. The corresponding oxidation rate was 7.7 mg (SO_4^{2-})/kg/day when the molar ratio of gaseous O_2 consumption to SO_4^{2-} production based on the stoichiometry of the pyrite oxidation reaction was 1.75:1.0 (Hollings et al., 2001). The oxidation rate of the waste rock in Column 1 (waste rock without cover) was higher than that in Test 1. Since O_2 did not limit waste rock oxidation in Test 1, based on the observed O_2 concentrations in Fig. 4 (except during the period of precipitation), the above mentioned difference in oxidation rates between Column 1 and Test 1 may be attributed to the effect of water flushing. This observation is consistent with the findings of Song and Yanful (2008) who reported that partially covered waste rock oxidized less than the uncovered waste rock due to reduced flushing and, consequently, limited availability of fresh sulfide-bearing mineral surfaces for oxidation.

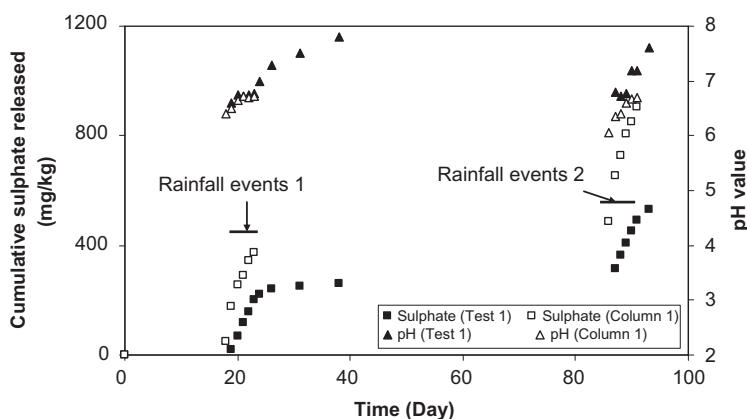


Fig. 9. Measured pH and calculated cumulative SO_4^{2-} from measured SO_4^{2-} concentrations in the percolate water in Test 1 (waste rock with channelled cover) and in Column 1 (waste rock without cover).

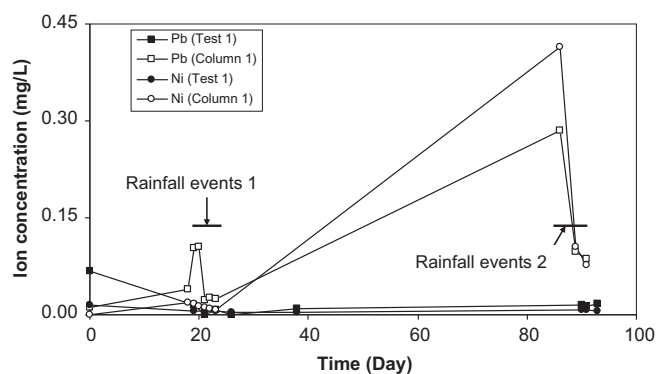


Fig. 10. Measured ion concentrations of Pb and Ni in the percolate water in Test 1 (waste rock with channelled cover) and in Column 1 (waste rock without cover).

The measured concentrations of Pb and Ni in the percolate water in Column 1 were generally much higher than those in Test 1, especially after the long drying period (Day 85) as shown in Fig. 10. For example, the measured Pb concentrations in Column

1 were 0.02–0.29 mg/L and 0.01–0.41 mg/L for Ni, while during the same period the measured concentration in Test 1 was less than 0.02 mg/L for Pb (the detection limit was 0.01 mg/L for Pb) and less than 0.01 mg/L for Ni (with a detection limit of 0.01 mg/L). These results are in agreement with the measured pH values and released cumulative SO_4^{2-} . The lower contaminant metal concentrations (e.g. Pb, Ni) in the percolate water in Test 1 might be attributed to (1) the lower oxidation rate of the waste rock in Test 1; (2) the higher pH of the percolate water in Test 1, which could have enhanced metal precipitation. The difference in scales of Test 1 and Column 1 could also produce variations in the measured ion concentrations in the percolate waters obtained from Test 1 and Column 1, because of possible difference in flow patterns. An attempt has been to minimise the impact of this variation in the analysis by normalizing the cumulative SO_4^{2-} release from the two set-ups with respect to the mass of waste rock (mg/kg) used in each experiment (Fig. 9).

Table 3 presents average metal concentrations measured in the percolate waters from Test 1 and Column 1. In general, most alkaline and alkaline earth metals had higher concentrations in Test 1 than in Column 1. Some metals, such as Ca, K and Na, had higher concentration in Test 1 than in Column 1 probably due to their

Table 3
Measured metal(loid) concentrations in the percolate water from Test 1 and Column 1.

Metal ion	Test 1 ^a		Column 1 ^b	
	Mean (mg/L)	Standard deviation (mg/L)	Mean (mg/L)	Standard deviation (mg/L)
Al	1.34×10^{-2}	7.80×10^{-4}	6.08×10^{-2}	4.61×10^{-2}
Sb	9.60×10^{-3}	5.95×10^{-3}	6.99×10^{-3}	2.63×10^{-3}
As	6.95×10^{-3}	1.03×10^{-3}	1.25×10^{-2}	7.96×10^{-3}
Ba	1.26×10^{-2}	7.50×10^{-3}	7.58×10^{-3}	2.65×10^{-3}
Cd	7.10×10^{-4}	3.90×10^{-4}	5.18×10^{-2}	8.24×10^{-2}
Ca	5.60×10^2	5.99×10^1	4.89×10^2	1.39×10^2
Co	1.82×10^{-3}	5.80×10^{-4}	2.72×10^{-2}	4.99×10^{-2}
Cu	7.66×10^{-3}	6.44×10^{-3}	1.49×10^{-2}	1.74×10^{-2}
Fe	9.16×10^{-2}	5.49×10^{-2}	2.04×10^{-1}	2.26×10^{-1}
Pb	1.25×10^{-2}	3.78×10^{-3}	8.77×10^{-2}	8.21×10^{-2}
Mg	7.11×10^1	1.81×10^1	1.26×10^2	1.96×10^2
Mn	3.13×10^0	1.30×10^0	8.17×10^0	1.56×10^1
Ni	5.80×10^{-3}	1.36×10^{-3}	7.43×10^{-2}	1.32×10^{-1}
K	2.38×10^1	7.90×10^0	6.19×10^0	2.63×10^0
Se	4.94×10^{-3}	3.63×10^{-3}	1.30×10^{-1}	8.72×10^{-2}
Si	3.54×10^1	3.79×10^0	2.78×10^1	6.72×10^0
Na	1.92×10^1	8.06×10^0	8.93×10^0	5.06×10^0
Sr	1.09×10^0	1.64×10^{-1}	7.42×10^{-1}	3.06×10^{-1}
Zn	4.92×10^{-1}	5.91×10^{-1}	2.43×10^1	5.35×10^1

^a Test 1: Waste rock with channelled cover.

^b Column 1: Waste rock without cover.

leaching from the overlying soil cover layers (mainly, the sand layer). The mineralogical analysis and Toxicity Characteristic Leaching Procedure (TCLP) (USEPA, 1992) tests indicated that Ca was much more abundant in the sand and silty clay than in the waste rock. The measured metal (Al, Cd, Zn, Cu, Fe and Mn) concentrations were higher in Column 1 than in Test 1. This difference in percolate water quality was due to the reduced oxidation of the covered waste rock (Test 1) and the higher pH of the leachate from the overlying sand layer. However, over the monitoring period (5 months) of the experiments, only Zn concentration in the percolate water (24.3 mg/L) from the uncovered waste rock exceeded the Metal Mining Effluent Regulations (MMER) (Environment Canada, 2006).

Table 4 presents the minerals that potentially controlled the chemistry of the final percolate waters and their saturation indices (SI values) as predicted by PHREEQC. Aluminum concentrations were likely controlled by Al_2O_3 and amorphous $\text{Al}(\text{OH})_3$ in Column 1 and by boehmite and gibbsite in Test 1, based on the SI values. The concentration of SO_4^{2-} was likely controlled by barite and gypsum in Column 1 and Test 1. Percolate water from Test 1 was supersaturated with respect to ferrihydrite and saturated with respect to $\text{Fe}_3(\text{OH})_8$, while percolate water from Column 1 was supersaturated with respect to ferrihydrite and schwertmannite. Goethite and lepidocrocite also had the potential to form in both tests. Thus these minerals likely influenced Fe concentrations in the percolate water in both tests. Potassium concentration was likely controlled by K-jarosite in Test 1 and Column 1. In general, Table 4 indicates that most minerals controlling dissolved species concentrations in the percolate water in Test 1 were similar to those in Column 1 due to the similar environment in both tests. However, the difference in pH and metal concentrations in the percolate waters due to the different oxidation rates of the waste rock

in Test 1 and Column 1 and the addition of leached dissolved ions from the overlying cover layers in Test 1 likely had some effect on the types of minerals controlling the percolate water chemistry.

4. Discussion

The half-life used in the modeling to account for the decrease in O_2 concentration due to O_2 consumption in the waste rock was 0.005 a, which meant the corresponding bulk O_2 decay coefficient (the optimum bulk O_2 decay coefficient) was 0.38 day^{-1} . This value was less than the bulk O_2 decay coefficient (0.67 day^{-1}) calculated from the measured SO_4^{2-} release rate in Column 1 using the equation proposed by Song and Yanful (2010c). In this calculation, the volumetric water content used to estimate the effective porosity of the waste rock was 0.145, the average oven dry volumetric water content measured at the end of the test. The discrepancy between the optimum and calculated bulk O_2 decay coefficient could be attributed to the measured SO_4^{2-} release rate in Column 1. The measured SO_4^{2-} release indicated that the waste rock in Column 1 had a larger SO_4^{2-} release rate than in Test 1. When the SO_4^{2-} release rate ($5.0 \text{ mg } (\text{SO}_4^{2-})/\text{kg}/\text{day}$) measured in Test 1 was used, the calculated bulk O_2 decay coefficient was 0.40 day^{-1} , which is close to the bulk O_2 decay coefficient obtained from the program calibration. This suggests that the Song and Yanful (2010c) method of using the SO_4^{2-} release rate to estimate the bulk O_2 decay coefficient gives reasonable values if a reliable SO_4^{2-} release rate is used. Using the SO_4^{2-} release rate to calculate the O_2 decay coefficient, as in the present study, provides a reasonable method to estimate an initial O_2 decay coefficient for O_2 concentration modeling. Moreover, the oxidation rate of the waste rock expressed as the SO_4^{2-} release rate can be easily obtained from a humidity cell test, which has become a routine test in mine rock identification (Price, 2005). If the oxidation rate ($7.7 \text{ mg } (\text{SO}_4^{2-})/\text{kg}/\text{day}$) obtained from the modeled O_2 influx (102 g over 151 days) was used, the calculated bulk O_2 decay coefficient would be 0.6 day^{-1} , which is slightly larger than the optimum value (0.38 day^{-1}). However, the bulk O_2 decay coefficient can still be used to obtain a reasonable initial estimate of O_2 concentration in the waste rock if the oxidation rate is not available.

The sensitivity analysis indicated that changing the location of the channel pathway would have greater effect on O_2 flux than changing the saturated hydraulic conductivity of the channel material. However, the relationship between the modeled O_2 fluxes and the saturated hydraulic conductivity of the channel material showed that even a relatively small saturated hydraulic conductivity (2.4 m/day) of the channel material could cause a considerable amount of O_2 to flux into the underlying waste rock and compromise cover performance. Thus measures should be taken in soil cover design and construction to prevent the development of macropores in barrier layers. Otherwise, repairs must be undertaken quickly to prevent increased O_2 ingress from the macropores to the underlying mine waste. The modeled cases indicate that the part of the waste rock that was close to the channel pathway had a relatively large O_2 concentration compared to farther locations. This result may be employed to identify the location of the channel pathways or other macropores developed in barrier layers in soil covers. For example, if a waste rock pile underlying a soil cover is divided into many small square cells, and O_2 sensors are installed in each cell to monitor the O_2 concentration, then it would not be too difficult to locate macropores that can potentially transport significant quantities of O_2 into the waste rock pile through the measured O_2 concentration contour. Some mapping technologies and optimization methods may facilitate the analysis of the measured O_2 concentration contours to quickly locate the position of the macropores.

Table 4

Minerals potentially controlling the chemistry of percolate waters from Test 1 (covered waste rock) and Column 1 (uncovered waste rock) and their saturation indices predicted by PHREEQC.

Minerals	Formula	Test 1 ^a	Column 1 ^b
$\text{Al}(\text{OH})_3$ (am) ^c		-2.0	-0.45
Al_2O_3		-2.1	0.99
$\text{Al}_4(\text{OH})_{10}\text{SO}_4$		-4.2	3.7
Alunite	$\text{KAl}_3(\text{SO}_4)_2(\text{OH})_6$	-2.7	3.8
Anglesite	PbSO_4	-2.9	-1.6
Anhydrite	CaSO_4	-0.32	-0.31
Barite	BaSO_4	0.56	0.11
Boehmite	AlOOH	0.22	1.8
Celestite	SrSO_4	-1.1	-1.4
Chalcedony	SiO_2	0.68	0.41
Cristobalite	SiO_2	0.48	0.21
$\text{Cu}(\text{OH})_2$		-2.5	-2.0
Cuprite	Cu_2O	-3.8	-2.7
CuSe		1.3	3.9
Diaspore	AlOOH	2.0	3.5
$\text{Fe}_3(\text{OH})_8$		-0.18	-4.6
Ferrihydrite	$\text{Fe}(\text{OH})_3$	2.8	1.2
Gibbsite	$\text{Al}(\text{OH})_3$	0.55	2.1
Goethite	FeOOH	5.6	4.0
Gypsum	$\text{CaSO}_4 \cdot 2\text{H}_2\text{O}$	-0.06	-0.04
K-Jarosite	$\text{KFe}_3(\text{SO}_4)_2(\text{OH})_6$	2.3	-0.65
Lepidocrocite	$\text{FeO}(\text{OH})$	4.9	3.2
Na-Jarosite	$\text{NaFe}_3(\text{SO}_4)_2(\text{OH})_6$	-1.5	-4.3
$\text{Pb}(\text{OH})_2$		-1.5	-1.9
Quartz	SiO_2	1.1	0.86
SbO_2		-1.2	-0.80
Schwertmannite	$\text{Fe}_8\text{O}_8(\text{OH})_6\text{SO}_4$	12	1.9
Tenorite	CuO	-1.5	-0.95
Zincite	ZnO	-1.7	-2.1

^a Test 1: Waste rock with channelled cover.

^b Column 1: Waste rock without cover.

^c am means amorphous.

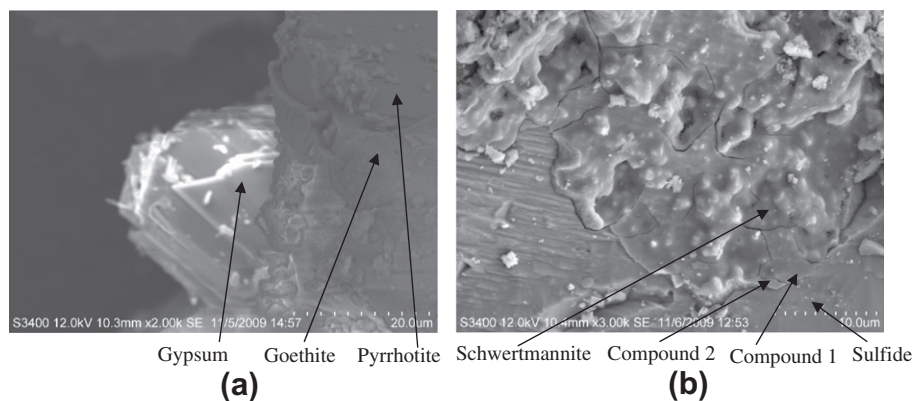


Fig. 11. SEM images of waste rock samples obtained in Test 1 (a) and in Column 1 (b) after experiments indicate that gypsum and goethite are present in the waste rock sample in Test 1 and schwertmannite is present in Column 1. Compounds 1 and 2 are minerals with Fe, O and S elements. Compound 1 has 14% O (weight percentage) and Compound 2 has 28% O. Sulfide comprises pyrite (major part) and pyrrhotite.

Based on SEM–EDX analysis, goethite and gypsum were found to be the secondary minerals present in the waste rock sample obtained in Test 1 after test (Fig. 11a), and schwertmannite could be present in the waste rock sample obtained from Column 1 after test (Fig. 11b). It was also found, from the SEM–EDX analysis, that O_2 contents increase with distance from the unoxidized face of the waste rock sample obtained from Column 1 (after test), suggesting that the oxidation of the waste rock may be consistent with the shrinking core model (Davis and Ritchie, 1986; Ritchie, 2003; Molson et al., 2005). Goethite was considered more likely to form than lepidocrocite in Test 1 because goethite is more stable than lepidocrocite (Schwertmann and Taylor, 1977). The reason that PHREEQC predicted a higher SI value for goethite is that a lower solubility constant ($\log K_{so}$) value (0.491) of goethite was used in the Minteq v4 database. Bigham et al. (1996) reported that the $\log K_{so}$ value for goethite was 1.4. If the $\log K_{so}$ of goethite were changed to 1.4 in PHREEQC, the predicted SI values for goethite would be 4.6 in Test 1. The lower solubility constant increased the predicted saturation index under the same conditions. The calculated formulae for schwertmannite present in the waste rock sample in Column 1 (Fig. 11b) after the test was $Fe_8O_8(OH)_{4.8}(SO_4)_{1.6} \cdot 6.7H_2O$, which is in the range of the schwertmannite formula, $Fe_{16}O_{16}(OH)_x(SO_4)_y \cdot nH_2O$ with $16 - x = 2y$ and $2.0 \leq y \leq 3.5$ (Bigham et al., 1994). Sensitivity analysis indicated that the PHREEQC predicted SI values of schwertmannite greatly depended on its formula, and less dependent on electron activity of the percolate water.

5. Conclusions

Tests involving mine waste rock underlying a soil cover with a channel flow pathway (Test 1) and waste rock without a cover (Column 1) were performed in the laboratory. The commercial finite element program VADOSE/W was calibrated and used to model the O_2 transport in Test 1, and the computer program PHREEQC was used to predict the possible secondary minerals in the percolate waters from both Test 1 and Column 1. The study focused on O_2 transport and geochemistry of the percolate water. Based on the results, the following conclusions may be drawn:

- (1) Waste rock closest to the channel (preferential flow pathway) had higher O_2 concentrations than waste rock in the periphery, indicating that the channel in the barrier layer was a major passage for O_2 ingress into the underlying waste rock. This finding may help to locate channel or preferential flow pathways that form in barrier layers in soil covers.

- (2) Modeling of O_2 concentrations in the waste rock layer underlying the soil cover with channel indicated that the actual flushing condition was an important factor when estimating the O_2 decay coefficient from measured SO_4^{2-} release rate.
- (3) Oxygen ingress into the waste rock underlying the soil cover with channel was more sensitive to the location of the channel than to the saturated hydraulic conductivity of the channel filling material.
- (4) The waste rock underlying the soil cover with channel oxidized less than the uncovered waste rock due to less flushing, implying a fractured or channelled cover with preferential flow can still mitigate ARD to some extent.
- (5) Minerals controlling percolate water chemistry in Column 1 were similar to those in Test 1 because of similar environments in the two tests. Gypsum possibly influenced SO_4^{2-} concentrations in the percolate water in both tests. Ferrihydrite, goethite, lepidocrocite, and schwertmannite likely controlled Fe concentration in both tests. SEM–EDX confirmed the formation of gypsum and goethite in the waste rock with the channelled soil cover and schwertmannite in the uncovered waste rock.

Acknowledgements

Funding for this research has been provided by the Natural Sciences and Engineering Research Council of Canada in the form of an Individual Discovery Grant awarded to E.K. Yanful.

References

- Adu-Wusu, C., Yanful, E.K., 2006. Performance of engineered test covers on acid-generating waste rock at Whistle mine, Ontario. *Can. Geotech. J.* 43, 1–18.
- Aubertin, M., Aachib, M., Authier, K., 2000. Evaluation of diffusive gas flux through covers with a GCL. *Geotext. Geomembr.* 18, 215–233.
- Aubertin, M., Chapuis, R.P., Aachib, M., Ricard, J.-F., Tremblay, L., Bussière, B., 1994. Cover technology for acidic tailings: hydrogeological properties of milling wastes used as capillary barrier. In: Carrier W.D. (Ed.), *Proc. 1st Int. Congress on Environmental Geotechnique, ISSMFE-CGS*, Edmonton, pp. 427–432.
- Beven, K., Germann, P., 1982. Macropores and water flow in soils. *Water Resour. Res.* 18, 1311–1325.
- Bigham, J.M., Carlson, L., Murad, E., 1994. Schwertmannite a new iron oxyhydroxysulfate from Pyhäsalmi, Finland, and other localities. *Mineral. Mag.* 58, 641–648.
- Bigham, J.M., Schwertmann, U., Traina, S.J., Winland, R.L., Wolf, M., 1996. Schwertmannite and the chemical modeling of iron in acid sulfate waters. *Geochim. Cosmochim. Acta* 60, 2111–2121.
- Bussière, B., Aubertin, M., Chapuis, R.P., 2003. The behavior of inclined covers used as oxygen barriers. *Can. Geotech. J.* 40, 512–535.

- Bussière, B., Aubertin, M., Zhan, G., 2007. Discussion: "Design of inclined covers with capillary barrier effect" by S.-E. Parent and A. Cabral. *Geotech. Geol. Eng.* 25, 673–678.
- Collin, M., Rasmuson, A., 1988. A comparison of gas diffusivity models for unsaturated porous media. *Soil Sci. Soc. Am. J.* 52, 1559–1565.
- Davis, G.B., Ritchie, A.I.M., 1986. A model of oxidation in pyritic mine wastes: part 1 equations and approximate solution. *Appl. Math. Model.* 10, 314–321.
- Environment Canada, 2006. Status Report on Water Pollution Prevention and Control under the Metal Mining Effluent Regulations in 2003. EPS 1/MM/12, Environment Canada.
- GEO-SLOPE, 2004. VADOSE/W 2004 User's Guide. GEO-SLOPE International Limited, Calgary, Alberta.
- Germann, P., Beven, K., 1981. Water flow in soil macropores 1. An experimental approach. *J. Soil Sci.* 32, 1–13.
- Hill, D.E., Parlange, J.-Y., 1972. Wetting front instability in layered soils. *Soil Sci. Soc. Am. J.* 36, 697–702.
- Hollings, P., Hendry, M.J., Nicholson, R.V., Kirkland, R.A., 2001. Quantification of oxygen consumption and sulphate release rates for waste rock piles using kinetic cells: Cluff lake uranium mine, northern Saskatchewan, Canada. *Appl. Geochem.* 16, 1215–1230.
- Krahn, J., 2004. Vadose Zone Modeling with VADOSE/W: An Engineering Methodology. GEO-SLOPE International Ltd., Calgary, Alberta.
- Kung, K.-J.S., 1990. Preferential flow in a sandy vadose zone, 2, mechanisms and implications. *Geoderma* 46, 59–71.
- Majzlan, J., Navrotsky, A., Schwertmann, U., 2004. Thermodynamics of iron oxides: part III. Enthalpies of formation and stability of ferrihydrite ($\sim\text{Fe}(\text{OH})_3$), schwertmannite ($\sim\text{FeO}(\text{OH})_{3/4}(\text{SO}_4)_{1/8}$), and $\varepsilon\text{-Fe}_2\text{O}_3$. *Geochim. Cosmochim. Acta* 68, 1049–1059.
- MEND, 1991. Acid Rock Drainage Prediction Manual. MEND Project 1.16.1b. Coastech Research Inc., Vancouver, Canada.
- Molson, J.W., Fala, O., Aubertin, M., Bussière, B., 2005. Numerical simulations of pyrite oxidation and acid mine drainage in unsaturated waste rock piles. *J. Contam. Hydrol.* 78, 343–371.
- Nicholson, R.V., Gillham, R.W., Cherry, J.A., Reardon, E.J., 1989. Reduction of acid generation in mine tailings through the use of moisture-retaining layers as oxygen barriers. *Can. Geotech. J.* 26, 1–8.
- O'Kane, M., Wilson, G.W., Barbour, S.L., 1998. Instrumentation and monitoring of an engineered soil cover system for mine waste rock. *Can. Geotech. J.* 35, 828–846.
- Parkhurst, D.L., Appelo, C.A.J., 1999. User's guide to PHREEQC—a computer program for speciation, reaction path, 1d-transport and inverse geochemical calculation. *US Geol. Surv. Water-Resour. Invest. Rep.*, 99–4259.
- Price, W.A., 2005. List of Potential Information Requirements in Metal Leaching/Acid Rock Drainage Assessment and Mitigation Work. CANMET Mining and Mineral Sciences Laboratories, Natural Resources Canada. Division Report MMSL 04-040 (TR), MEND Report 5.10E.
- Ritchie, A.I.M., 2003. Oxidation and gas transport in piles of sulfidic material. In: Jambor, J.L., Blowes, D.W., Ritchie, A.I.M. (Eds.), *Environmental Aspects of Mine Wastes*. Short Course Series, vol. 31. Mineralogical Association of Canada, pp. 73–94.
- Schwertmann, U., Taylor, R.M., 1977. Iron oxides. In: Dixon, J.B. (Ed.), *Minerals in Soil Environments*. Soil Science Society of America, Madison, Wisconsin, USA, pp. 145–180 (Chapter 5).
- Selker, J.S., Steenhuis, T.S., Parlange, J.-Y., 1992. Wetting front instability in homogeneous sandy soils under continuous infiltration. *Soil Sci. Soc. Am. J.* 56, 1346–1350.
- Song, Q., Yanful, E.K., 2008. Monitoring and modeling of sand–bentonite cover for ARD mitigation. *Water Air Soil Pollut.* 190, 65–85.
- Song, Q., Yanful, E.K., 2010a. Effect of channelling on water balance, oxygen diffusion and oxidation rate in mine waste rock with an inclined multilayer soil cover. *J. Contam. Hydrol.* 114, 43–63.
- Song, Q., Yanful, E.K., 2010b. Laboratory and numerical modeling of water balance in a layered sloped soil cover with channel flow pathway over mine waste rock. *Environ. Earth Sci.* doi:10.1007/s12665-010-0488-4.
- Song, Q., Yanful, E.K., 2010c. Effect of water addition frequency on oxygen consumption in acid generating waste rock. *J. Environ. Eng. ASCE* 136, 691–700.
- Stormont, J.C., 1996. The effectiveness of two capillary barriers on a 10% slope. *Geotech. Geol. Eng.* 14, 243–267.
- Taylor, G., Spain, A., Nefiodovas, A., Timms, G., Kuznetsov, V., Benntt, J., 2003. Determination of the Reasons for Deterioration of the Rum Jungle Waste Rock Cover. Australian Center for Mining Environmental Research, Brisbane.
- USEPA, 1992. Method 1311. Toxicity Characteristic Leaching Procedure. Test Methods for Evaluating Solid Wastes Physical/Chemical Methods. United States Environmental Protection Agency, Washington, DC.
- USEPA, 1994. Acid Mine Drainage Prediction. Technical Document (EPA530-R-94-036). US Environmental Protection Agency, Office of Solid Waste, Special Waste Branch, Washington, DC.
- USEPA, 1999. MINTEQA2/PRODEFA2, A Geochemical Assessment Model for Environmental Systems: User Manual Supplement for Version 4.0. US Environmental Protection Agency, National Exposure Research Laboratory, Ecosystem Research Division, Athens, Georgia.
- Walter, M.T., Kim, J.-S., Steenhuis, T.S., Parlange, J.-Y., Heilig, A., Braddock, R.D., Selker, J.S., Boll, J., 2000. Funneled flow mechanisms in a sloping layered soil: laboratory investigation. *Water Resour. Res.* 36, 841–849.
- Weeks, B., Wilson, G.W., 2005. Variations in moisture content for a soil cover over 10 year period. *Can. Geotech. J.* 42, 1615–1630.
- Woyshner, M.R., Yanful, E.K., 1995. Modelling and field measurements of water percolation through an experimental soil cover on mine tailings. *Can. Geotech. J.* 32, 601–609.
- Yanful, E.K., 1993. Oxygen diffusion through soil covers of sulphidic mine tailings. *J. Geotech. Eng.* 119, 1207–1228.
- Yanful, E.K., Mousavi, S.M., Yang, M., 2003. Modeling and measurement of evaporation in moisture-retaining soil covers. *Adv. Environ. Res.* 7, 783–801.
- Zehe, E., Flüßler, H., 2001. Preferential transport of isoproturon at a plot scale and a field scale tile-drained site. *J. Hydrol.* 247, 100–115.